FULL PAPER

ADVANCED
ENERGY
MATERIALS

www.advenergymat.d

Check for
updates

Revealing and Elucidating ALD-Derived Control of Lithium Plating Microstructure

Solomon T. Oyakhire, William Huang, Hansen Wang, David T. Boyle, Joel R. Schneider, Camila de Paula, Yecun Wu, Yi Cui,* and Stacey F. Bent*

The practical implementation of Li metal batteries is hindered by difficulties in controlling the Li metal plating microstructure. While previous atomic layer deposition (ALD) studies have focused on directly coating Li metal with thin films for the passivation of the electrode–electrolyte interface, a different approach is adopted, situating the ALD film beneath Li metal and directly on the copper current collector. A mechanistic explanation for this simple strategy of controlling the Li metal plating microstructure using TiO_2 grown on copper foil by ALD is presented. In contrast to previous studies where ALD-grown layers act as artificial interphases, this TiO_2 layer resides at the copper–Li metal interface, acting as a nucleation layer to improve the Li metal plating morphology. Upon lithiation of TiO_2, a Li_xTiO_2 complex forms; this alloy provides a lithiophilic surface layer that enables uniform and reversible Li plating. The reversibility of lithium deposition is evident from the champion cell (5 nm TiO_2), which displays an average Coulombic efficiency (CE) of 96% after 150 cycles at a moderate current density of 1 mA cm^{-2}. This simple approach provides the first account of the mechanism of ALD-derived Li nucleation control and suggests new possibilities for future ALD-synthesized nucleation layers.

1. Introduction

Lithium-ion batteries have transformed energy storage and are prevalent across a wide range of consumer electronics. However, batteries with increased energy densities are required for electrical grids and electric vehicles in today's renewable energy transition.[1–6] In comparison to conventional anodes, lithium metal possesses a higher gravimetric capacity (3860 mAh g^{-1}) and lower reduction potential (−3.04 V), making lithium metal batteries (LMBs) ideal candidates for energy-intensive infrastructure.[7] Unfortunately, lithium metal is plagued by numerous morphological instabilities that result in the destruction of the solid electrolyte interphase (SEI) and formation of dendrites[8–10] as shown in **Figure 1**a. To address the fallibilities of lithium metal, numerous strategies have been employed, ranging from designing electrolytes to reduce the number of side reactions between lithium and the electrolyte,[11–14] engineering hosts that accommodate and control the expansion of lithium,[15–21] and, in some very recent cases, to incorporating artificial SEIs that passivate the interface between lithium metal and the electrolyte.[22–37]

Of all the modern strategies employed to passivate lithium metal, artificial SEIs positioned at the Li–electrolyte interface have shown some of the most promising results. Materials such as polymers,[25–27] inorganic metal oxides,[27–29] inorganic nitrides,[30] fluorides,[31–33] nanodiamond,[34] and hybrid structures[35,36] have been applied as interfacial layers, and for the most part, they support uniform plating and stripping of lithium by passivating the reactive Li surface against the electrolyte. In the formation of artificial SEIs, the use of techniques that ensure conformality at the interface is key, and as a result, there is a predilection for the use of atomic layer deposition (ALD) and molecular layer deposition (MLD). Both ALD and MLD are techniques based on sequential and self-limiting surface reactions that result in uniform films. Literature reports have shown immense potential for ALD-grown and MLD-grown artificial SEIs ranging from the use of alumina,[28,29] alucone,[35] polyurea,[37] and, more recently, to alternating stacked layers of alucone and alumina,[36] resulting in improved performance of lithium metal batteries. Yet, because most artificial

S. T. Oyakhire, J. R. Schneider, C. de Paula, Prof. S. F. Bent
Department of Chemical Engineering
Stanford University
Stanford, CA 94305, USA
E-mail: sbent@stanford.edu
W. Huang, H. Wang, Prof. Y. Cui
Department of Materials Science and Engineering
Stanford University
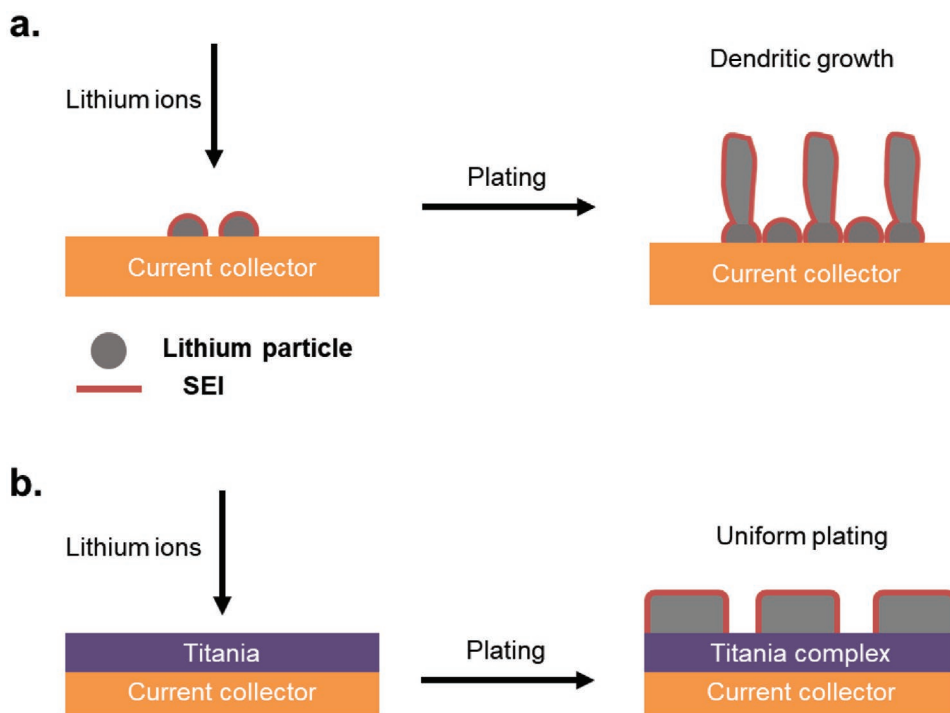Stanford, CA 94305, USA
E-mail: yicui@stanford.edu
D. T. Boyle
Department of Chemistry
Stanford University
Stanford, CA 94305, USA
Y. Wu
Department of Electrical Engineering
Stanford University
Stanford, CA 94305, USA
Prof. Y. Cui
Stanford Institute for Materials and Energy Sciences
SLAC National Accelerator Laboratory
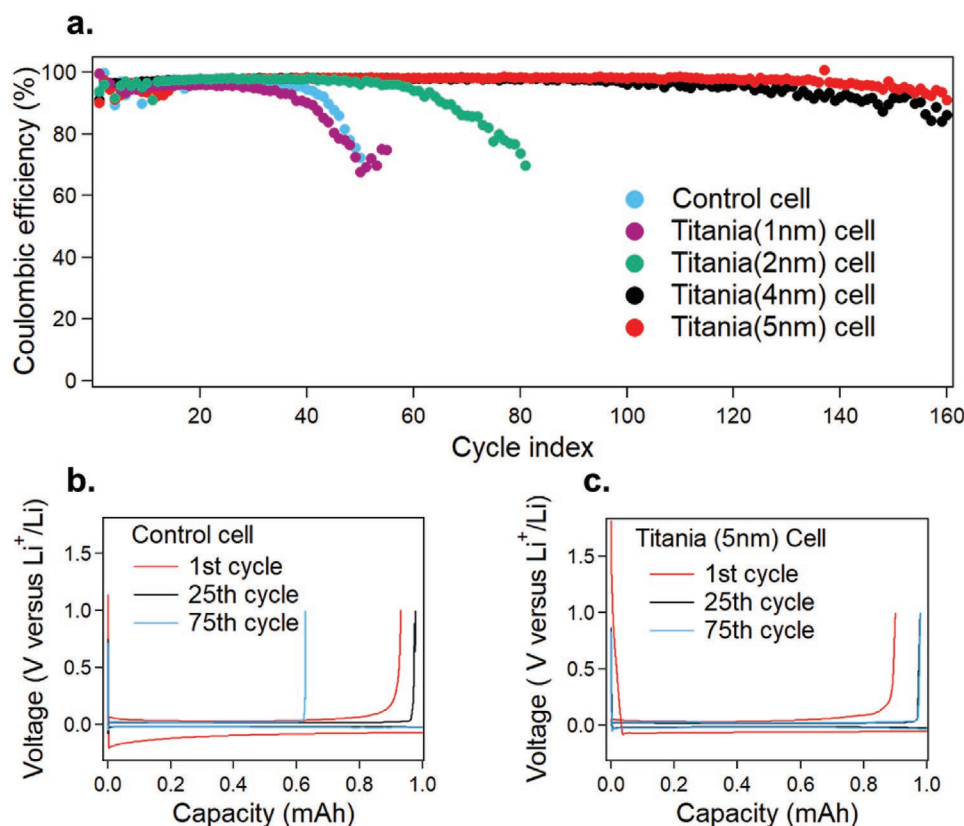Menlo Park, CA 94025, USA

2002736 (1 of 11)

Figure 1. Schematic of lithium plating on different substrates. a) Uncontrolled nucleation and formation of dendrites during growth of lithium on pristine current collector. b) Controlled nucleation and uniform growth of lithium on TiO_2-modified current collector. Illustrations of lithium nucleation are simplified.

SEI materials are inherently insulating, the consistent need for lithium ions to shuttle across them during cycling results in their fracture and eventual delamination. To address this limitation, it is pertinent to reconsider the design principles vis à vis the location of these interfacial materials in electrochemical cells.

Rather than using ALD to grow artificial SEIs, a relatively unexplored design is to use ALD to grow nucleation control layers that remain at the current collector–Li interface to tune Li metal plating morphology. Addressing the nucleation behavior of lithium is crucial for ensuring high performance in LMBs. The commonly used current collector for lithium nucleation is copper, which is lithiophobic, implying that it presents a high energy barrier for the nucleation of lithium.[19,30,38,39] This high nucleation barrier (overpotential) has been shown to foster the formation of small and densely distributed lithium particles, leading to an increase in electrolyte contact surface area, quick formation of dendrites, and subsequent cell failure.[38,40] Previous methods for controlling lithium metal nucleation such as the use of zero overpotential metallic seeds (Ag and Au) are expensive.[19,41] Controlling the nucleation of Li on Cu without sacrificing its energy density requires careful chemical synthesis and design, and we posit that surface modification of the Cu current collector by the deposition of a thin nucleation layer may yield a promising low-cost approach for improved Li metal morphology.

Here, we present a study that involves an unconventional use of ALD-grown TiO_2 as a nucleation layer for lithium metal, rather than as an artificial SEI (Figure 1b). While artificial SEIs lie at the Li–electrolyte interface, our TiO_2 layer remains fixed at the current collector–Li interface. By depositing TiO_2

directly on the copper current collector, rather than on top of lithium, we can control the nucleation morphology of lithium metal in a commonly used ether electrolyte. TiO_2 possesses properties that may be beneficial toward Li plating morphology. TiO_2 has a high dielectric constant,[42] suggesting that it could foster the dissolution of lithium ions from the anionic spheres of the electrolyte, thereby homogenizing the flux and growth of lithium. TiO_2 also reacts favorably with lithium to form Li_2O and Ti, as evidenced by the change in free energy of the reaction at room temperature ($\Delta G = -233.6$ kJ mol^{-1}).[43] Based on previous reports, lithium nucleates easily when it first forms alloys or compounds with other elements.[19] As such, we hypothesize that the reaction of lithium with TiO_2 will result in the formation of a complex mixture of Li_2O and Ti that lowers the energy barrier for further lithium nucleation. As has been previously demonstrated, a low energy barrier is correlated with the creation of large lithium particles, and an improvement in cell performance.[44] While a recent report by Tan et al.[45] has demonstrated TiO_2 for Li metal stabilization, the origins of this stabilization and its role as a nucleation layer are not understood in depth.[45] We demonstrate that in the presence of a range of ALD-grown TiO_2 thicknesses, lithium nucleates into larger deposits under significantly reduced overpotential, possibly resulting in a reduction in its contact surface area with the electrolyte, culminating in an increase in cell performance. In addition, we report substantial improvements in cycling efficiency and reversibility over extended cycles in Li/Cu cells. Using X-ray photoelectron spectroscopy (XPS), scanning electron microscopy (SEM), energy dispersive X-ray spectroscopy (EDS), and transmission

ADVANCED
SCIENCE NEWS

www.advancedsciencenews.com

ADVANCED
ENERGY
MATERIALS

www.advenergymat.de

Figure 2. Improved electrochemical performance of TiO_2-modified cells demonstrated using Li/Cu cells. All cells were cycled in DOL/DME/LiNO$_3$ with 1.0 M LiTFSI salt at a current density of 1 mA cm^{-2}. a) CE of Li/Cu cells cycled with pristine copper, and copper modified with 1, 2, 4, and 5 nm of TiO_2, respectively. b,c) Voltage profiles of b) the Li/Cu cells at different cycle indices for the control cell, and c) for the 5 nm TiO_2-modified cell.

electron microscopy (TEM), we propose mechanistic explanations for the role of TiO_2 as a nucleation layer on the copper foil and establish the origin of the TiO_2 film's effect. The use of ALD for the growth of this TiO_2 nucleation layer ensures conformality, creates room for scalability, and provides control over nanoscale parameters that impact performance without compromising energy density. This work reveals a new area of study for nanoscale films in lithium metal stabilization and creates opportunities for synergistic combinations with existing lithium metal passivation principles.

2. Results and Discussion

2.1. Electrochemical Cycling Using Lithium–Copper Cells

To verify the impact of TiO_2 on Li metal cycling, we test Coulombic efficiency (CE) in Li/Cu cells with a common ether-based electrolyte used in Li/S batteries and for Li metal characterization, 1.0 M lithium bis(trifluoromethanesulfonyl) imide (LiTFSI) in 1:1 v:v 1,3 dioxolane (DOL)/1,2-dimethoxyethane (DME) with 1 wt% lithium nitrate (LiNO$_3$) additive (DOL/DME/LiNO$_3$). Unaided, the DOL/DME/LiNO$_3$ electrolyte usually fails (CE < 80%) after 50 cycles when cycled at room temperature,[44] and its failure is usually correlated with the consumption of the anionic nitrate component in its SEI.[44]

The control cell in our study is composed of pristine copper cycled against lithium metal, and its performance is in direct agreement with literature, failing at a cycle index of 50 when cycled at a current density of 1 mA cm^{-2} (**Figure 2**a). To identify the optimal thickness of the TiO_2 nucleation layer, we utilize Cu foils ALD-coated with TiO_2 films of thicknesses 1, 2, 4, 5, and 10 nm. We observe from Figure 2a that 1 nm TiO_2 shows a similar CE trend as the control cell, likely due to incomplete coverage of the Cu foil at such a low thickness of TiO_2. At such low thicknesses, metal oxide films are typically isolated islands rather than fully coalesced films.[46] The 2 nm TiO_2 film shows slight improvement over the control and 1 nm cells, displaying signs of failure after 65 cycles, indicating improved coverage over Cu (Figure 2a). Interestingly, in the presence of thicker layers of TiO_2, improvements to cycle life of the Li/Cu cells are very significant; the 4 and 5 nm titania cells are cycled to about 150 cycles with an average CE of 96% before they begin to show signs of capacity fade (Figure 2a). The 10 nm film also shows some promise as evidenced by its extended cyclability (Figure S1, Supporting Information); however, it shows a first cycle CE of 76%, calling its practical use into question. To ensure that our observations are not artifacts, we verify the performance of the 4 and 5 nm TiO_2 cells using at least two cells and find that they are reproducible (Figures S2 and S3, Supporting Information).

Furthermore, we examine the voltage profiles in the 1st, 25th, and 75th cycles to characterize the early, mid-stage, and

late-stage reversibility of the control cell and the 5 nm TiO_2-modified cell. From Figure 2b, in the control cell, the first cycle reveals significant loss of lithium ($\approx 10\%$), and this could be ascribed to the formation of an SEI. Using a total plating capacity of 1 mAh cm^{-2}, the 25th cycle of the control cell reveals almost complete reversibility during stripping with a capacity of 0.9761 mAh cm^{-2}. However, the 75th stripping cycle shows a very significant decrease in cycling reversibility, with only 62.7% of the plated capacity retrieved during stripping. This cycling behavior provides evidence that corroborates the CE plot presented in Figure 2a, indicating that the pristine copper foil does not support long-term reversible plating and stripping of lithium. The tendency of pristine Cu to display low cycling reversibility can be attributed to its reported high lithium nucleation barrier.[38] A high nucleation barrier promotes the formation of small lithium particles[39] with high nuclei density and electrolyte contact area, leading to an increase in the loss of lithium to unwanted electrolyte reactions and a reduction in cycling reversibility. This continuous electrolyte reaction results in the continuous buildup of SEI and impedance, leading to eventual cell failure.[47]

In sharp contrast, the 5 nm TiO_2-modified cell reveals outstanding reversibility. From Figure 2c, we observe that the 5 nm TiO_2 cell displays a stripping capacity of 0.89 mAh cm^{-2}, indicating an 11% loss in the first cycle plating capacity of lithium. This loss in lithium could be attributed to the formation of SEI and could also suggest an irreversible reaction between lithium and TiO_2 during the first cycle of plating. However, upon further cycling, the voltage profile shows almost complete extraction of plated lithium in the mid-stage and late-stage cycles. We observe little capacity loss in the 25th and 75th electrochemical cycles, with the cell maintaining a stripping capacity of 0.979 mAh cm^{-2} (Figure 2c). The tendency of TiO_2 to improve the reversibility of lithium plating and stripping may be attributed to the thermodynamically favorable reactions between lithium and TiO_2 leading to the formation of a lithium-rich compound that makes nucleation more energetically favorable. A reduction in nucleation energy barrier could promote the formation of large lithium particles with reduced electrolyte contact area, leading to a reduction in the loss of lithium to unwanted electrolyte reactions and improved reversibility of lithium stripping.[44]

In a bid to probe the efficacy of this TiO_2 nucleation layer in other electrolyte systems, we examine its performance in a conventional carbonate electrolyte free of $LiNO_3$, 1 M lithium hexafluorophosphate ($LiPF_6$) in 1:1 v/v ethylene carbonate/diethyl carbonate (EC/DEC) with 10 wt% fluoroethylene carbonate (FEC) and 1 wt% vinylene carbonate (VC). Our experiments show that cell performance in the presence of this electrolyte is not substantially improved by addition of TiO_2 (Figure S4, Supporting Information). This result suggests that the mechanism by which TiO_2 improves performance relies on the favorable SEI kinetics and stable interphase conferred by the $LiNO_3$ additive in the DOL/DME electrolyte.[44] Since the DOL/DME electrolyte is speculated to fail when the nitrate component in the electrolyte is fully consumed,[44] our results suggest that the presence of TiO_2 as a nucleation layer slows down its consumption. This also agrees with our reversibility argument which hinges on the formation of lithium particles having lower

contact area with the electrolyte. By reducing the contact area with the electrolyte, the amount of lithium lost to reactions with the electrolyte is reduced, and the consumption of nitrate in the electrolyte is reduced, resulting in the improved reversibility in stripping and plating shown in Figure 2a–c.

2.2. Deriving Insights from Nucleation Studies

To further investigate the improved performance of the 5 nm TiO_2 cell over the control cell, we analyze the first cycle lithiation potential curves of the Li/Cu cells. Lithiation potential curves are useful for providing information about the nucleation overpotential, a parameter defined as the difference between the potential at which nucleation is initiated and that at which the nucleated lithium particles grow. This nucleation overpotential reflects the energy barrier that must be surpassed for the lithium particles to grow and is a significant factor in determining the performance of Li/Cu cells.[44] In the presence of 5 nm TiO_2, the nucleation overpotential reduces from 129.5 to 20.2 mV at a current density of 1 mA cm^{-2}, indicating a lower nucleation energy barrier in the presence of TiO_2 (**Figure 3**a). This reduction in nucleation overpotential is present across all thicknesses of titania, as shown in Figure 3b. The 1 nm TiO_2 layer provides a very small reduction in overpotential in comparison to pristine copper because TiO_2 does not cover the copper surface at such small thicknesses; at angstrom levels of thickness, thin films are expected to exist as islands rather than fully coalesced films.[46] Furthermore, as we increase the thickness of TiO_2 from 2 to 5 nm, we observe a corresponding decrease in nucleation overpotential, indicating that the coverage of the copper foil becomes more complete within that thickness range (Figure 3b). However, we observe that the 10 nm film causes an increase in nucleation overpotential in comparison to the 5 nm film (Figure 3b). One possible explanation for this observation is that as thickness increases, the electronic resistance of the thin film begins to approach its bulk value. As a result, it could become more difficult for electrons from the external circuit to tunnel through the film to support the reduction of lithium ions on top of the film during nucleation.

Studies have shown that nucleation overpotential and the critical radius of lithium nuclei are inversely proportional.[39,44] Hence, to understand how our observed disparities in nucleation overpotential affect deposition morphology, we carry out SEM studies to visualize the morphology of lithium after the first cycle of plating. We perform SEM studies of the cells at a fixed current density of 1 mA cm^{-2} with capacities of 0.1, 0.3, and 1 mAh cm^{-2} to capture the effect of nucleation on final Li particle size.

Comparing the control and 5 nm TiO_2 cells in earlier stages of lithium growth, collected after 0.3 mAh cm^{-2} of lithium plating, we observe differences in particle size, with the TiO_2-modified cell forming bigger particles (Figure 3c,d). The isolated nuclei of lithium formed on the pristine copper at the early stages of growth (Figure 3c) are attributed to poor affinity between Li adatoms and Cu, causing lithium embryos to remain fixed after nucleation.[40] On the contrary, the presence of TiO_2 enables the coalescence of nucleated adatoms (Figure 3d), suggesting that lateral growth of Li particles becomes more favorable. We also
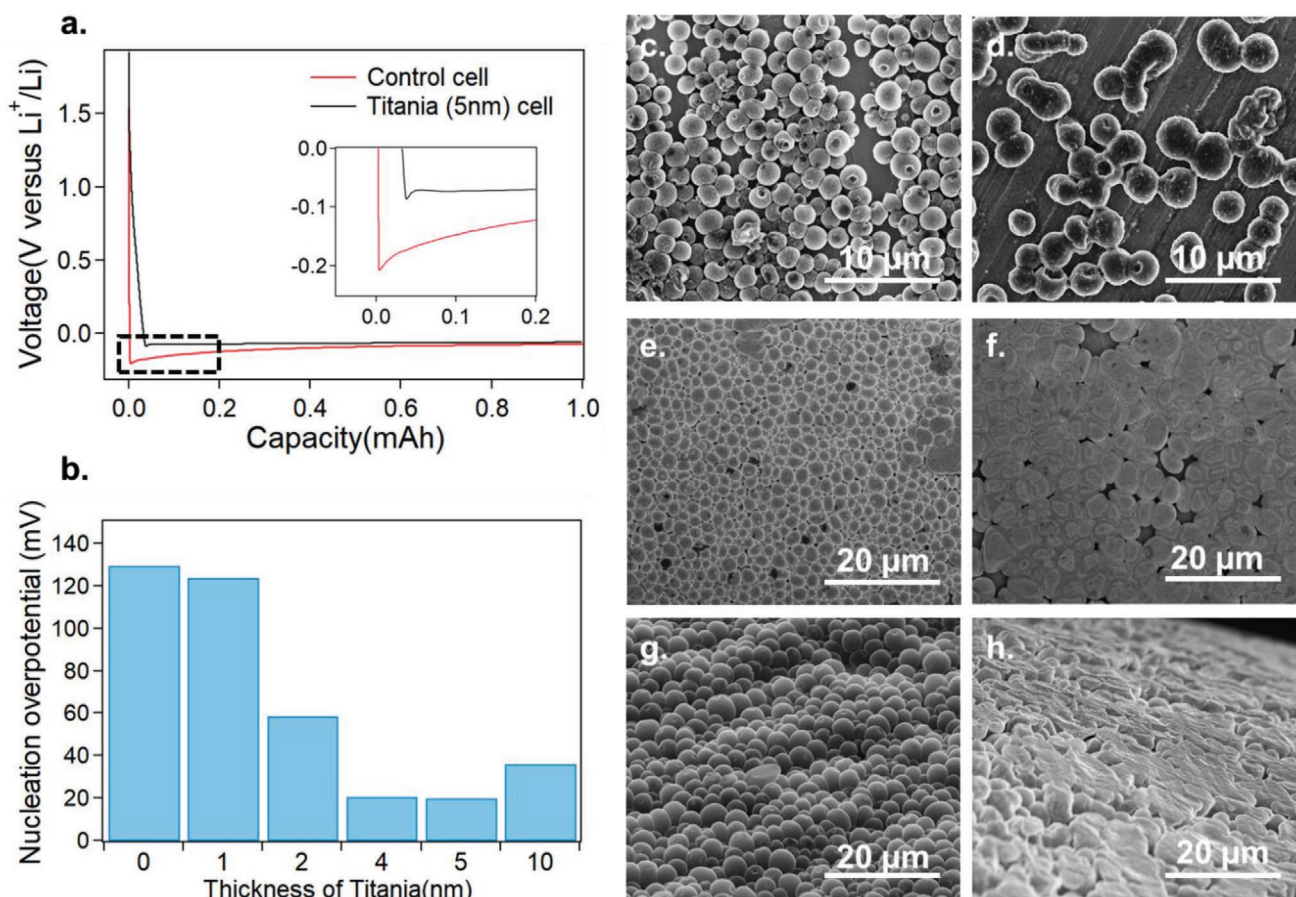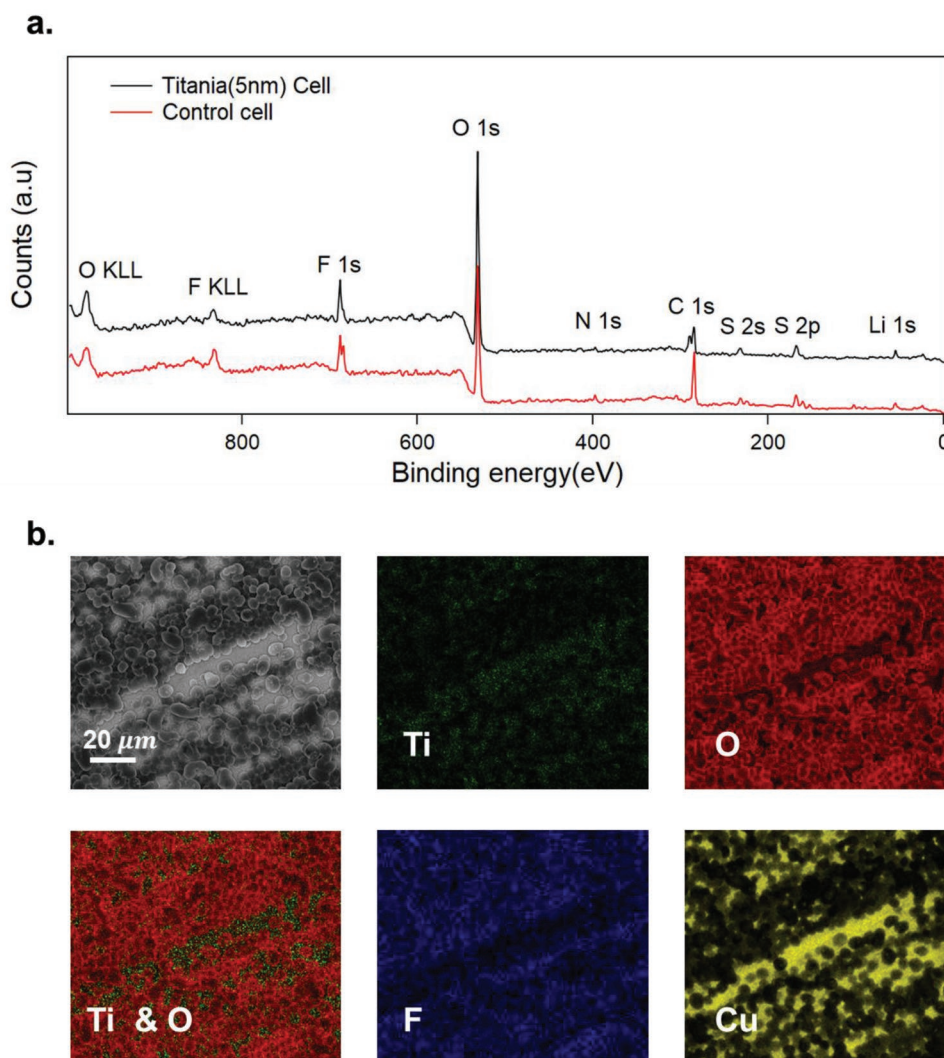
Figure 3. TiO$_2$-modified cells reduce nucleation overpotential and promote formation of larger lithium nucleates. a) First cycle plating voltage profiles for control cell and 5 nm TiO$_2$ cell at a current density of 1 mA cm^{-2}. Inset: enlarged image of boxed region showing nucleation potential differences more clearly. b) First cycle nucleation overpotential as a function of thickness of TiO$_2$. c,d) Top-view SEM images of 0.3 mAh cm^{-2} lithium embryos formed in the control cell and 5 nm TiO$_2$ cell, respectively. e,f) Top-view SEM images of 1 mAh cm^{-2} lithium particles formed in the control cell and 5 nm TiO$_2$ cell, respectively. g,h) Cross-sectional SEM images of 1 mAh cm^{-2} lithium embryos formed in the control cell and 5 nm TiO$_2$ cell, respectively, with samples tilted at about 30° to the horizontal. All cells were cycled at a current density of 1 mA cm^{-2}.

detect similar trends at an even lower plating capacity of 0.1 mAh cm^{-2} (Figure S5, Supporting Information).

In Figure 3e,f, we plate 1 mAh cm^{-2} of lithium on top of pristine copper and 5 nm TiO$_2$, respectively. From Figure 3e, we observe that the average diameter of the lithium particles in the control cell is 2 µm, and there appears to be close packing of the small particles, while in the presence of 5 nm titania, the average diameter of the particles is 5 µm in a similarly packed structure (Figure 3f). This similarity in packing structure and difference in average particle diameter between the 5 nm TiO$_2$ and pristine Cu cells show that the areal nuclei density of lithium is reduced in the presence of TiO$_2$. This implies that, for the same capacity of deposited lithium, the pristine cell has more exposed surface area, thereby increasing particle contact with the electrolyte. Cross-sectional SEM carried out on samples tilted at about 30° to the horizontal reveals the disparity in nucleation properties even more clearly. For 1 mAh cm^{-2} of lithium on pristine copper, Figure 3g shows that lithium is present in spheres with high nuclei density, while Figure 3h taken at the same capacity of lithium on 5 nm TiO$_2$ shows lower nuclei density and planar rather than spherical deposits.

We hypothesize that the planar and larger deposits formed in the presence of 5 nm TiO$_2$ facilitate a reduction in the exposed surface area of lithium nucleates, and as a result, lead to a significant reduction in the rate of nitrate consumption in the electrolyte. And because the rate of consumption of nitrate in this electrolyte corresponds to how quickly it fails, it follows that the 5 nm TiO$_2$ results in extended cycling of the cell with improved reversibility of plating and stripping. To verify that the effect of the TiO$_2$ is to change the lithium morphology via the chemical changes it undergoes during plating, and not an effect of smoothing of the Cu substrate, we perform atomic force microscopy (AFM) on copper and TiO$_2$-modified copper before electrochemical cycling. We find no significant difference in roughness between the TiO$_2$-modified and pristine copper (Figure S6, Supporting Information). This indicates that the change in lithium nucleation morphology is induced by the chemical effects conferred by TiO$_2$. Titania's improvement in electrochemical performance could also be ascribed to the stabilization of copper against electrolyte decomposition before lithium plating. However, immediately after lithium is exposed to the electrolyte during plating, it becomes the main

ADVANCED
SCIENCE NEWS
www.advancedsciencenews.com

ADVANCED
ENERGY
MATERIALS
www.advenergymat.de

Figure 4. Chemical characterization reveals that TiO_2 remains atop the Cu current collector during cycling. a) Survey scan of the control cell and 5 nm TiO_2 cell after plating with 50 µAh cm^{-2} of lithium. b) SEM-EDS mapping of 0.6 mAh cm^{-2} of plated Li on the 5 nm TiO_2 cell (secondary electron image top left) showing the distribution of elemental species on Li and Cu foil.

contributor to electrolyte decomposition. As a result, the reduction in lithium surface area through morphological changes conferred by TiO_2 most likely contributes more significantly to the improvement in cell performance.

2.3. Chemical Role of TiO_2

Substantiating the role of TiO_2 requires the verification of its location in the electrochemical cell; as a nucleation layer, TiO_2 would remain atop the copper foil after lithium deposition, but as an artificial SEI, TiO_2 would support the diffusion of Li through it, and thus sit atop Li. These two roles would create very different chemical speciation at the electrode–electrolyte interface. For a nucleation layer, we would expect the electrode–electrolyte interface to be filled with SEI components obtained from electrolyte reduction, while in the case of an artificial SEI, one would anticipate an electrode–electrolyte interface

populated by TiO_2, the SEI. To verify the chemical role of TiO_2, we carry out XPS on the control and 5 nm TiO_2 cells, each plated with 50 µAh cm^{-2} of Li, in order to examine the composition at the electrode–electrolyte interface. The probing depth limit of XPS ($\approx$10 nm) ensures that we capture the elemental composition only at the electrode–electrolyte interface. From the survey scan in **Figure 4**a, we observe that in both the control and 5 nm TiO_2 cells, the elemental species that are present at the interface are F, O, N, C, S, and Li, corresponding to the elemental make-up of an SEI formed by the reduction of components of the DOL/DME/$LiNO_3$ electrolyte. This indicates that in both the control cell and the 5 nm TiO_2 cell, Li metal maintains contact with the electrolyte after plating, resulting in the supply of electrons to the electrolyte for SEI formation. In addition, we observe the complete absence of Ti, which has a binding energy of 458.5 eV in TiO_2, at the electrode–electrolyte interface of the 5 nm TiO_2 cell (Figure 4a) supporting that TiO_2 does not act as an artificial SEI. Because the Li beneath

**ADVANCED
SCIENCE NEWS**

www.advancedsciencenews.com

**ADVANCED
ENERGY
MATERIALS**

www.advenergymat.de

the SEI is ≈250 nm thick, we do not see the Ti signal from the underlying TiO_2 nucleation layer since that film is buried beneath Li. From the survey scan, there is an apparent difference in C and F peaks between both cells, and while we do not probe this any further because of the spatial variations in the composition of the SEI, we acknowledge that there may be additional benefits to electrochemical performance induced by the differences in decomposition products. In addition to the survey scan, we carry out a depth profile on the TiO_2-modified cell that reveals Ti signals after 1 min of sputtering (Figure S7, Supporting Information). However, we refrain from drawing in-depth insights from the depth-profile feature of XPS because it does not completely capture in-plane heterogeneities, especially when sensitive materials are analyzed.[48]

To further verify the chemical role of TiO_2, we perform SEM–EDS mapping of 0.6 mAh cm^{-2} of Li plated on a 5 nm TiO_2-modified cell. SEM–EDS affords us the ability to visualize the surface of the plated Li, as well as the Cu foil regions that remain exposed after plating. Figure 4b shows the SEM image of the plated Li, in addition to the net count of elemental signals from Ti, O, F, and Cu. By virtue of the high reactivity and low electrochemical redox potential of lithium versus standard hydrogen,[7] it is within reason to assume that the surface of Li is covered by the SEI-reduced species from the electrolyte. The SEI derived from the DOL/DME electrolyte used in this study has been shown to contain O signal, obtained from the reduction of the solvents (DOL and DME), and F signal,[49] originating from the halide-laden salt (LiTFSI). Because Li signals cannot be directly detected within the windowed EDS detectors, we use the O and F signals as indicators for the SEI and the Li surface, respectively. O and F signals show high net counts on regions that are fully covered by lithium, with weak counts on the exposed Cu surface (Figure 4b). While Cu does form an SEI, the thickness is less than that of the SEI on Li, resulting in weaker O and F EDS signals relative to that of the Li deposit.[50] Given the thickness of the Li layer (3 μm), the X-ray signal arising from the Cu current collector can only be observed in regions that are not covered by Li; these regions are seen in the Cu elemental mapping image in Figure 4b. Notably, the Ti signals are only present in regions that are not covered by Li metal (depicted by Cu signals), indicating that Ti remains atop Cu, rather than on top of Li. Also, as shown in the overlay of O and Ti signals in Figure 4b, the Ti signals do not overlap with the strong O signals, clearly suggesting that TiO_2 remains distinct from the Li SEI. A similar finding was recently reported in which Al_2O_3 remains beneath Li after plating.[51] In the same vein, our SEM–EDS findings further corroborate the XPS results, which suggest that TiO_2 supports the nucleation of Li while remaining atop Cu and is not incorporated into the SEI.

2.4. Understanding the Nucleation Mechanism of TiO₂

Modifying the nucleation energy barrier of Li metal is typically associated with "lithiophilicity," which is defined as the ability of a material to react in a stable manner with Li.[18] To probe the lithiophilicity of TiO_2, we examine the first cycle Li plating

profiles for the control cell and TiO_2-modified cells. The Li plating profiles in Li/Cu cells allow us to identify the capacity of Li lost before nucleation begins. The sloping voltage profile of the 5 nm TiO_2 cell during plating in Figure 3a reveals Faradaic behavior before the onset of nucleation at –70 mV, indicating that Li (≈0.01 mAh cm^{-2}) is consumed above the Li plating potential. Because this phenomenon is not observed in the control cell (Figure 3a), we repeat the study for TiO_2-modified cells of different thicknesses to derive some understanding (**Figure 5**a).

It is evident that an increase in the thickness of TiO_2 results in an increasingly sloping potential profile and an increase in the 0 V capacity of the modified cells. This observation suggests that some of the lithium ions shuttled toward the copper foil react with TiO_2 before nucleation begins as evidenced by the increase in capacity of Li lost before the onset of nucleation, and as such, as the amount of TiO_2 increases, the quantity of lithium that reacts prior to nucleation increases. We also note that this type of potential profile has been observed in studies where Li reacts with the nucleation layer.[47] A quantitative analysis of this phenomenon, described in the following sections, provides further evidence that lithium is reacting with TiO_2.
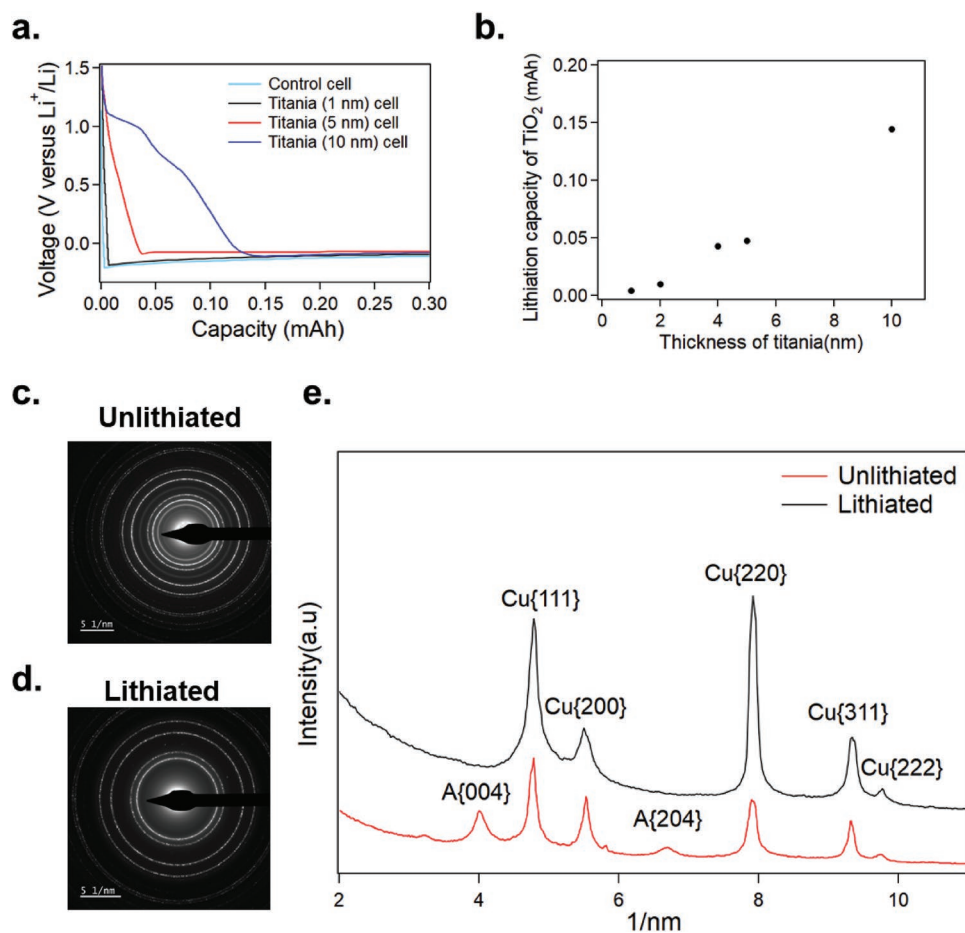
By discounting the plating capacity lost before lithiation in the control cell, we roughly estimate the prenucleation plating capacity of lithium lost in the reaction with TiO_2 using the following equation

$$Q_{titania} = Q_{coated} - Q_{uncoated} \tag{1}$$

where $Q_{titania}$ is the capacity of lithium lost toward reaction with TiO_2, Q_{coated} is the capacity of lithium lost prenucleation in the TiO_2-modified cells, and $Q_{uncoated}$ is the capacity of lithium lost prenucleation in the pristine copper cells.

This sort of coulometry assumes a constant SEI capacity in both cells, which may not be the case. As a result, we refrain from relying on its absolute results; rather, we choose to draw qualitative insights from the trend that it presents. Figure 5b shows an increase in the uptake of lithium (in the form of prenucleation capacity lost) as the thickness of TiO_2 increases. Because there is a near-linear relationship between prenucleation Li uptake and TiO_2 thickness, this result strongly indicates that lithium reacts with TiO_2 to form a complex mixture such as Li_xTiO_2. This observation is in agreement with previous studies on the use of TiO_2 as an anode material in Li-ion batteries in which the formation of Li_xTiO_2 was identified as the charging mechanism.[52,53] Moreover, this result is expected because lithium reacts with TiO_2 in a thermodynamically favorable process.[43]

To gain insights into the structure of this Li_xTiO_2 complex, we perform ALD of TiO_2 on a Cu-coated C film TEM grid and assemble half cells using the TEM grid as the working electrode. Using cryogenic TEM methods[44,54,55] to prevent any air reaction with the lithiated TiO_2, we carry out electron diffraction on pristine and lithiated TiO_2 films. The electron diffraction pattern on the pristine TiO_2 in Figure 5c shows the characteristic rings associated with the nanocrystallites of TiO_2 and the crystal planes of copper upon which TiO_2 was deposited. However, the diffraction pattern of the lithiated film contains fewer

**ADVANCED
SCIENCE NEWS**

www.advancedsciencenews.com

**ADVANCED
ENERGY
MATERIALS**

www.advenergymat.de

Figure 5. Lithium reacts with TiO_2 to form an amorphous Li_xTiO_2 complex. a) Voltage profiles for first cycle of lithium plating for control cell, 1, 5, and 10 nm TiO_2 cells. b) Lithium uptake as a function of thickness of TiO_2. c,d) Electron diffraction patterns for unlithiated and lithiated TiO_2, respectively. e) Lateral intensity profile from c,d) for unlithiated and lithiated TiO_2, where A represents the anatase phase of TiO_2.
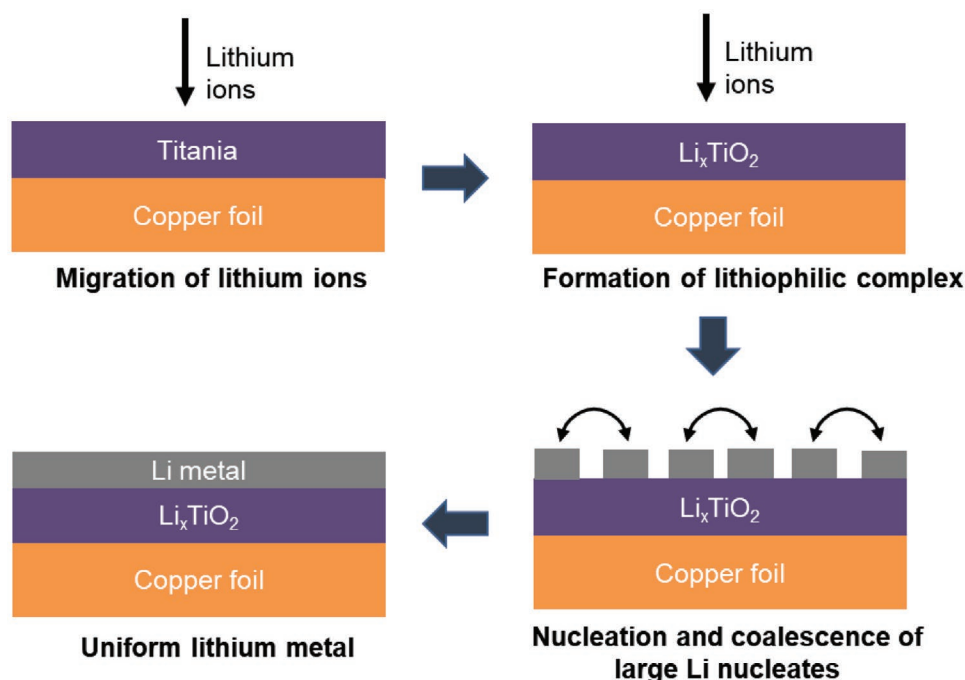
rings as shown in Figure 5d. Translating the diffraction patterns into a lateral intensity profile, we observe that the anatase peaks associated with TiO_2 (labeled A) are present in the pristine film but are notably absent in the lithiated film, indicating that the nanocrystalline phase of TiO_2 is lost upon reaction with lithium (Figure 5e). Also, peaks corresponding to pure Li_2O are not detected. This result is consistent with production of a Li_xTiO_2 complex that is amorphous. The amorphous nature of the Li_xTiO_2 may contribute to the ease of Li nucleation; a recent study revealed that vacancies in lithium titanium oxide structures can increase their electronic conductivity.[56]

Combining insights from these characterization tools, we propose a mechanistic explanation describing the location and role of TiO_2 in its regulation of lithium morphology, as shown schematically in **Figure 6**. During the diffusion/migration of lithium ions from the counter electrode under a concentration gradient and an electric potential difference, the lithium ions that first reach the TiO_2 film react to form a Li_xTiO_2 complex. By virtue of the presence of this lithium "alloy," subsequent reduction of lithium ions takes place at lower overpotential, resulting in the formation of large and planar particles of lithium. This Li_xTiO_2 complex may also have more favorable wetting properties to Li metal leading to larger Li particle sizes and improved

continuity of the plated lithium metal. The resulting large and planar particles of lithium reduce the surface area of Li and consequently reduce electrolyte consumption and SEI degradation, while also increasing the reversibility of Li plating and stripping. Further studies should be carried out to better understand the fundamental nucleation phenomena at the interface of the Li_xTiO_2 complex. Given the strong enhancement in lithium metal battery's performance suggested by the present work, the results also suggest investigations into other ALD-grown materials that could be applied as nucleation layers in LMBs.

3. Conclusions

We have shown and provided a mechanistic explanation for a method of controlling the deposition morphology of lithium metal using an ALD-grown TiO_2 nucleation layer. By tuning the thickness of TiO_2 at the nanoscale, we reveal that the cyclability of lithium metal in DOL/DME/$LiNO_3$ electrolyte can be improved significantly. Using a current density of 1 mA cm^{-2}, we report an average Coulombic efficiency of 96% after 150 cycles in the champion 5 nm titania-modified cell with voltage profiles that reveal improved cyclability in

**ADVANCED
SCIENCE NEWS**
www.advancedsciencenews.com

**ADVANCED
ENERGY
MATERIALS**
www.advenergymat.de

Figure 6. Schematic illustration of the role of TiO_2 as a nucleation layer for electrodeposited lithium. SEI not depicted for simplicity.

the early, mid, and late cycle stages of Li/Cu cells. TiO_2 in the champion cell modifies the deposition morphology of lithium metal by eliciting a reduction in its nucleation overpotential, resulting in larger lithium nucleates. We propose that the larger lithium particles result in a reduction in the contact surface area between lithium metal and the electrolyte thus diminishing the rate of electrolyte degradation. Using coulometry and electron diffraction, we demonstrate that the TiO_2 film reacts with Li to form an amorphous Li_xTiO_2 complex. This complex remains at the Li–current collector interface and serves as a nucleation layer, rather than as an artificial SEI, and likely increases the surface lithiophilicity, supporting continuous reversible stripping and plating of lithium metal with minimal consumption of SEI components. In sum, we have presented the first account of the mechanistic details for the effect of an ALD-grown nucleation layer on Li plating and resolved the common misconception that Li always deposits beneath ALD-grown films after lithiation. This study provides a framework for investigating Li nucleation and opens a new range of opportunities for tuning the nucleation morphology of lithium metal at the nanoscale using ALD-grown inorganic metal oxides such as CuO and ZnO, and we posit that this ability to limit the consumption of SEI components could be especially useful if combined synergistically with electrolytes that are engineered to form stable SEIs leading to high-performing lithium metal batteries.

4. Experimental Section

TiO_2 Film Deposition: For ALD TiO_2 deposition, titanium isopropoxide (TTIP), heated to 60 °C, was the metal–organic precursor and water (H_2O) was the counter reactant. The depositions were conducted

directly on Cu foil in a Gemstar 6 ALD reactor (Arradiance). An ALD scheme of 5/30/2/30 s TTIP pulse/purge/H_2O pulse/purge sequence at 150 °C was adopted, which provided for a growth rate of 0.3 Å per cycle. The TiO_2 thicknesses were determined by TiO_2 growth on a reference Si wafer, using a J.A. Woollam M2000 Variable Angle Spectroscopic Ellipsometer at 65° and 70° angles of incidence and wavelengths ranging from 210 to 1688 nm.

Electrochemistry: Type 2032 coin cells were assembled in an argon glovebox with a polymer separator (Celgard 2325). Li metal foil (0.75 mm thick, 99.9% Alfa Aesar) was used as the counter/reference electrode, and a Cu foil was used as the working electrode. This Li/Cu configuration was used for cyclability, SEM, and XPS characterizations. For the electron diffraction experiments, a Cu TEM grid with an amorphous carbon film was used as the working electrode. Two electrolytes were used, namely, 1.0 M LiTFSI in 1:1 vol/vol DOL/DME with 1% $LiNO_3$ (by weight) additive, and 1.0 M $LiPF_6$ in 1:1 vol/vol EC/DEC with 10% FEC and 1% VC additives. 75 μL of electrolyte was used in both instances.

All experiments were carried out at a current density of 1 mA cm^{-2}. Cycling experiments were conducted at a capacity of 1 mAh cm^{-2} while SEM plating experiments were carried out at capacities of 0.1, 0.3, and 1 mAh cm^{-2}. XPS plating experiments were carried out at a capacity of 50 μAh cm^{-2}.

XPS Characterization: Cu foil working electrodes were prepared in an Ar glovebox and rinsed with 90 μL of DME to remove residual Li salts, then transferred to an XPS chamber using a vacuum transfer vessel. XPS signals were collected on a PHI VersaProbe 1 scanning XPS microprobe with an Al Kα source.

Microscopy: All samples were rinsed with DME and dried inside the Ar glovebox before microscopy. For cryo-TEM analysis, samples were plunge frozen in liquid nitrogen without air exposure, in accordance with previous reports.[54] Samples were loaded onto a Gatan 626 cryogenic TEM holder under liquid nitrogen and maintained at −175 °C within the TEM column. Electron diffraction characterizations were carried out using an FEI Titan 80–300 environmental (scanning) TEM operated at an accelerating voltage of 300 kV. The instrument was equipped with an aberration corrector in the objective lens, which was tuned before each sample analysis. Selected area electron diffraction was carried out at a camera length of 1.2 m using a Gatan OneView camera. Scanning electron microscopy was performed using an FEI Magellan 400 XHR.

Supporting Information

Supporting Information is available from the Wiley Online Library or from the author.

Acknowledgements

Conflict of Interest

The authors declare no conflict of interest.

Author Contributions

S.T.O. and W.H. contributed equally to this work. S.T.O., W.H., Y.C., and S.F.B. conceived the idea and designed the experiments. S.T.O. performed ALD, electrode fabrication, and electrochemical measurements. S.T.O. and H.W. carried out XPS experiments. W.H., S.T.O., and C.P. performed SEM experiments. W.H. and Y.W. carried out electron diffraction measurements. D.T.B. assisted with electrochemical measurements. J.R.S. assisted with ALD. S.T.O., W.H., Y.C., and S.F.B. wrote the manuscript. All authors discussed the results and commented on the manuscript.

Data Availability

The data that support the findings in this study are available from the corresponding author upon reasonable request.

Keywords

[1] J. B. Goodenough, K. S. Park, *J. Am. Chem. Soc.* **2013**, *135*, 1167.
[2] J. M. Tarascon, M. Armand, in *Materials for Sustainable Energy: A Collection of Peer-Reviewed Research and Review Articles from Nature Publishing Group* (Ed: V. Dusastre), World Scientific Publishing Co., Singapore **2010**, pp. 171–179.
[3] Y. Sun, N. Liu, Y. Cui, *Nat. Energy* **2016**, *1*, 16071.
[4] J. B. Goodenough, Y. Kim, *Chem. Mater.* **2010**, *22*, 587.
[5] C. K. Chan, H. Peng, G. Liu, K. McIlwrath, X. F. Zhang, R. A. Huggins, Y. Cui, *Nat. Nanotechnol.* **2008**, *3*, 31.
[6] S. Chu, Y. Cui, N. Liu, *Nat. Mater.* **2017**, *16*, 16.
[7] D. Lin, Y. Liu, Y. Cui, *Nat. Nanotechnol.* **2017**, *12*, 194.
[8] M. D. Tikekar, S. Choudhury, Z. Tu, L. A. Archer, *Nat. Energy* **2016**, *1*, 16114.
[9] W. Xu, J. Wang, F. Ding, X. Chen, E. Nasybulin, Y. Zhang, J. G. Zhang, *Energy Environ. Sci.* **2014**, *7*, 513.
[10] C. Yang, K. Fu, Y. Zhang, E. Hitz, L. Hu, *Adv. Mater.* **2017**, *29*, 1701169.
[11] J. Qian, W. A. Henderson, W. Xu, P. Bhattacharya, M. Engelhard, O. Borodin, J. G. Zhang, *Nat. Commun.* **2015**, *6*, 6362.
[12] X.-Q. Zhang, X.-B. Cheng, X. Chen, C. Yan, Q. Zhang, *Adv. Funct. Mater.* **2017**, *27*, 1605989.
[13] J. Zheng, M. H. Engelhard, D. Mei, S. Jiao, B. J. Polzin, J. G. Zhang, W. Xu, *Nat. Energy* **2017**, *2*, 17012.
[14] X. Fan, L. Chen, O. Borodin, X. Ji, J. Chen, S. Hou, T. Deng, J. Zheng, C. Yang, S. C. Liou, K. Amine, K. Xu, C. Wang, *Nat. Nanotechnol.* **2018**, *13*, 715.
[15] K.-H. Chen, A. J. Sanchez, E. Kazyak, A. L. Davis, N. P. Dasgupta, *Adv. Energy Mater.* **2019**, *9*, 1802534.
[16] G. Huang, J. Han, F. Zhang, Z. Wang, H. Kashani, K. Watanabe, M. Chen, *Adv. Mater.* **2019**, *31*, 1805334.
[17] Q. Yun, Y.-B. He, W. Lv, Y. Zhao, B. Li, F. Kang, Q.-H. Yang, *Adv. Mater.* **2016**, *28*, 6932.
[18] D. Lin, Y. Liu, Z. Liang, H. W. Lee, J. Sun, H. Wang, K. Yan, J. Xie, Y. Cui, *Nat. Nanotechnol.* **2016**, *11*, 626.
[19] K. Yan, Z. Lu, H. W. Lee, F. Xiong, P. C. Hsu, Y. Li, J. Zhao, S. Chu, Y. Cui, *Nat. Energy* **2016**, *1*, 1.
[20] H. Pan, J. Chen, R. Cao, V. Murugesan, N. N. Rajput, K. S. Han, K. Persson, L. Estevez, M. H. Engelhard, J. G. Zhang, K. T. Mueller, Y. Cui, Y. Shao, J. Liu, *Nat. Energy* **2017**, *2*, 813.
[21] C. Niu, H. Pan, W. Xu, J. Xiao, J. G. Zhang, L. Luo, C. Wang, D. Mei, J. Meng, X. Wang, Z. Liu, L. Mai, J. Liu, *Nat. Nanotechnol.* **2019**, *14*, 594.
[22] X. B. Cheng, R. Zhang, C. Z. Zhao, F. Wei, J. G. Zhang, Q. Zhang, *Adv. Sci.* **2016**, *3*, 1500213.
[23] N. W. Li, Y. X. Yin, C. P. Yang, Y. G. Guo, *Adv. Mater.* **2016**, *28*, 1853.
[24] L. Fan, Z. Guo, Y. Zhang, X. Wu, C. Zhao, X. Sun, G. Yang, Y. Feng, N. Zhang, *J. Mater. Chem. A* **2019**, *8*, 251.
[25] J. Lopez, D. G. Mackanic, Y. Cui, Z. Bao, *Nat. Rev. Mater.* **2019**, *4*, 312.
[26] L. Porcarelli, A. S. Shaplov, F. Bella, J. R. Nair, D. Mecerreyes, C. Gerbaldi, *ACS Energy Lett.* **2016**, *1*, 678.
[27] Z. Yu, D. G. Mackanic, W. Michaels, M. Lee, A. Pei, D. Feng, Q. Zhang, Y. Tsao, C. V. Amanchukwu, X. Yan, H. Wang, S. Chen, K. Liu, J. Kang, J. Qin, Y. Cui, Z. Bao, *Joule* **2019**, *3*, 2761.
[28] E. Kazyak, K. N. Wood, N. P. Dasgupta, *Chem. Mater.* **2015**, *27*, 6457.
[29] A. C. Kozen, C.-F. Lin, A. J. Pearse, M. A. Schroeder, X. Han, L. Hu, S.-B. Lee, G. W. Rubloff, M. Noked, *ACS Nano* **2015**, *9*, 5884.
[30] Y. Li, Y. Sun, A. Pei, K. Chen, A. Vailionis, Y. Li, G. Zheng, J. Sun, Y. Cui, *ACS Cent. Sci.* **2018**, *4*, 97.
[31] J. Zhao, L. Liao, F. Shi, T. Lei, G. Chen, A. Pei, J. Sun, K. Yan, G. Zhou, J. Xie, C. Liu, Y. Li, Z. Liang, Z. Bao, Y. Cui, *J. Am. Chem. Soc.* **2017**, *139*, 11550.
[32] D. Lin, Y. Liu, W. Chen, G. Zhou, K. Liu, B. Dunn, Y. Cui, *Nano Lett.* **2017**, *17*, 3731.
[33] Y. Lu, Z. Tu, L. A. Archer, *Nat. Mater.* **2014**, *13*, 961.
[34] Y. Liu, Y. K. Tzeng, D. Lin, A. Pei, H. Lu, N. A. Melosh, Z. X. Shen, S. Chu, Y. Cui, *Joule* **2018**, *2*, 1595.
[35] Y. Zhao, L. V. Goncharova, Q. Sun, X. Li, A. Lushington, B. Wang, R. Li, F. Dai, M. Cai, X. Sun, *Small Methods* **2018**, *2*, 1700417.
[36] Y. Zhao, M. Amirmaleki, Q. Sun, C. Zhao, A. Codirenzi, L. V. Goncharova, C. Wang, K. Adair, X. Li, X. Yang, F. Zhao, R. Li, T. Filleter, M. Cai, X. Sun, *Matter* **2019**, *1*, 1215.
[37] Y. Sun, Y. Zhao, J. Wang, J. Liang, C. Wang, Q. Sun, X. Lin, K. R. Adair, J. Luo, D. Wang, R. Li, M. Cai, T.-K. Sham, X. Sun, *Adv. Mater.* **2019**, *31*, 1806541.

[38] Y. Gu, H. Xu, X. Zhang, W. Wang, J. He, S. Tang, J. Yan, D. Wu, M. Zheng, Q. Dong, B. Mao, *Angew. Chem., Int. Ed.* **2019**, *58*, 3092.

[39] A. Pei, G. Zheng, F. Shi, Y. Li, Y. Cui, *Nano Lett.* **2017**, *17*, 1132.

[40] Y. J. Kim, S. H. Kwon, H. Noh, S. Yuk, H. Lee, H. soo Jin, J. Lee, J. G. Zhang, S. G. Lee, H. Guim, H. T. Kim, *Energy Storage Mater.* **2019**, *19*, 154.

[41] Z. Peng, J. Song, L. Huai, H. Jia, B. Xiao, L. Zou, G. Zhu, A. Martinez, S. Roy, V. Murugesan, H. Lee, X. Ren, Q. Li, B. Liu, X. Li, D. Wang, W. Xu, J. Zhang, *Adv. Energy Mater.* **2019**, *9*, 1901764.

[42] A. P. Alekhin, S. A. Gudkova, A. M. Markeev, A. S. Mitiaev, A. A. Sigarev, V. F. Toknova, *Appl. Surf. Sci.* **2010**, *257*, 186.

[43] G. Ou, Y. Xu, B. Wen, R. Lin, B. Ge, Y. Tang, Y. Liang, C. Yang, K. Huang, D. Zu, R. Yu, W. Chen, J. Li, H. Wu, L. M. Liu, Y. Li, *Nat. Commun.* **2018**, *9*, 1302.

[44] J. Wang, W. Huang, A. Pei, Y. Li, F. Shi, X. Yu, Y. Cui, *Nat. Energy* **2019**, *4*, 664.

[45] L. Tan, X. Li, T. Liu, X. Li, *J. Power Sources* **2020**, *463*, 228157.

[46] M. Ohring, *Materials Science of Thin Films*, Academic Press, San Diego, CA **2002**, pp. 357–415.

[47] B.-Q. Li, X.-R. Chen, X. Chen, C.-X. Zhao, R. Zhang, X.-B. Cheng, Q. Zhang, *Research* **2019**, *2019*, 4608940.

[48] W. Huang, H. Wang, D. T. Boyle, Y. Li, Y. Cui, *ACS Energy Lett.* **2020**, *5*, 1128.

[49] F. Shi, A. Pei, A. Vailionis, J. Xie, B. Liu, J. Zhao, Y. Gong, Y. Cui, *Proc. Natl. Acad. Sci. USA* **2017**, *114*, 12138.

[50] W. Huang, D. T. Boyle, Y. Li, Y. Li, A. Pei, H. Chen, Y. Cui, *ACS Nano* **2019**, *13*, 737.

[51] M. J. Zachman, Z. Tu, L. A. Archer, L. F. Kourkoutis, *ACS Energy Lett.* **2020**, *5*, 1224.

[52] B. L. He, B. Dong, H. L. Li, *Electrochem. Commun.* **2007**, *9*, 425.

[53] T. Song, U. Paik, *J. Mater. Chem. A* **2015**, *4*, 14.

[54] Y. Li, W. Huang, Y. Li, A. Pei, D. T. Boyle, Y. Cui, *Joule* **2018**, *2*, 2167.

[55] Y. Li, Y. Li, A. Pei, K. Yan, Y. Sun, C. L. Wu, L. M. Joubert, R. Chin, A. L. Koh, Y. Yu, J. Perrino, B. Butz, S. Chu, Y. Cui, *Science* **2017**, *358*, 506.

[56] M. Kick, C. Grosu, M. Schuderer, C. Scheurer, H. Oberhofer, *J. Phys. Chem. Lett.* **2020**, *11*, 2535.

2002736 (11 of 11)